DOI: 10.1478/AAPP.96S3A10

AAPP | Atti della Accademia Peloritana dei Pericolanti
Classe di Scienze Fisiche, Matematiche e Naturali
ISSN 1825-1242

Vol. 96, No. S3, A10 (2018)

BIFURCATIONS OF EQUILIBRIA IN A MATHEMATICAL MODEL FOR METAL GROWTH

DEBORAH LACITIGNOLA*

ABSTRACT. In this paper we focus on a morphochemical reaction-diffusion model for metal growth whose capability to support spatial patterns was essentially associated to the diffusion-driven instability of a specific system equilibrium, the equilibrium P_e. However, this model exhibits a rich multiplicity of other equilibria. We show that several bifurcations involving some of the many equilibria of the DIB model can affect the system spatial-organization properties by allowing for the existence of a subregion inside the P_e's Turing parameter space where the system trajectories can also tend towards a spatially homogeneous equilibrium and the existence of a region outside the P_e's Turing parameter space where spatial patterns can emerge.

1. Introduction

The revolutionary paper of Alan Turing (Turing 1952), in 1952, triggered a whole new field of mathematical investigations into pattern formation. From then on, reaction-diffusion systems have become the paradigm for models of spatial self-organization, increasingly allowing for stimulating research in the field of non-linear dynamics (Kapral and Showalter 1995; Murray 2003; Vanag 2004). So far, Turing's diffusion-driven instability is one of the leading mechanisms for spatial pattern formation in reaction-diffusion systems and the related Turing patterns have been the subject of extensive studies in a variety of applied contexts, e.g. Epstein (1997), De Wit (1999), Maini and Othmer (2001), Murray (2003), Malchow *et al.* (2008), Cross and Greenside (2009), and Sherratt (2012).

Among the others, electrochemistry has provided a fertile ground of action for the understanding of spatial organization phenomena since many experiments have shown that simple reaction mechanisms can be responsible for complex spatio-temporal patterns and that small changes in the reaction conditions can make the patterns reorganize. With the aim to rationalize, appropriately manipulate and control the emergence of specific chemical patterns in electrodepositon, in Bozzini *et al.* (2013), a novel reaction-diffusion system - the DIB model - was introduced and deeply discussed from the physico-chemical point of view. In respect to other models already existing in the electrochemical context, the DIB model is different for two key features: (i) the coupling of morphology (surface profile) and

surface chemistry (composition); (ii) an original, flexible and physically straightforward electrochemical source terms.

The DIB model has been the object of extensive investigations from the theoretical and numerical points of view, that have both revealed its interesting spatio-temporal dynamics and a good qualitative accordance with alloy electrodeposition experiments. In Lacitignola *et al.* (2015), conditions for Turing pattern formation have been derived and a class of oscillating pattern investigated, due to the interplay between Turing and Hopf instabilities; in Lacitignola *et al.* (2014) the system has been shown to support spiral waves as well as an interesting mechanism of spiral break-up; in Bozzini *et al.* (2015) a multiple scales method has been applied to study the evolution of the pattern shape and amplitude close to the marginal stability of the equilibria; in Lacitignola *et al.* (2018) the effects of cross-diffusion on pattern formation and selection have been analyzed and discussed; in Lacitignola *et al.* (2017) the effect on pattern formation of variations in the domain geometry has been investigated by considering the DIB model on a spherical domain.

These studies have highlighted that the rich phenomenology supported by the DIB model is essentially linked to the destabilization mechanisms of one of the system equilibria, the equilibrium P_e, that corresponds to a flat electrode surface from which corrugation and hence morphology can develop. In fact, different morphological classes of spatial patterns can be found in the P_e's Turing parameter space because the equilibrium P_e undergoes diffusion-driven instability; the emergence of spiral waves as well as a spiral break-up phenomenology are linked to the oscillatory behavior of the kinetics terms due to a super-critical Hopf bifurcation involving P_e; oscillatory spatio-temporal patterns can appear in the system dynamics, in the neighboring of the codimension-two Turing-Hopf bifurcation point, because of the interaction of the Turing and Hopf instabilities.

However, numerical investigations linked to a parameter estimation problem recently developed for the DIB model (Sgura *et al.* 2018), have revealed the following two interesting features in the system dynamics. (I) By suitably decreasing the value of a specific system parameter (the parameter A_2) a certain subregion in the P_e's Turing parameter space can be found, where random spatial perturbations of P_e do not lead system trajectories towards stationary spatial patterns but instead drive the system dynamics towards a spatially homogeneous equilibrium, different from P_e. The lower is the value of A_2 the larger is such region that instead tends to completely disappear for sufficiently high values of A_2. We associate this phenomenology (I) to the subregion I in the P_e's Turing parameter space. (II) Stationary spatial patterns can be found also outside the P_e's Turing parameter space and, more precisely in a specific Region II, just below the transcritical bifurcation line.

As the DIB model exhibits a multiplicity of equilibria (Lacitignola *et al.* 2015) and an interesting number of bifurcations can be found that impact on the number and on the stability properties of the equilibria, it is enough reasonable to think that the above peculiarities in the system dynamics can be explained in terms of bifurcations of equilibria different from P_e. The aim of this paper is hence to provide a theoretical explanation for the existence of both Regions I and II, respectively inside and outside the P_e's Turing parameter space.

The paper is organized as follows: in Section **2**, we introduce the DIB model. In Section **3**, we review the different mechanisms of destabilization of the spatially homogeneous equilibrium P_e; in Section **4** we show that the existence and the features of the above Region

I can be explained by investigating the role played by the parameter A_2 on the system dynamics; in Section **5**, we show that Region II, corresponding to the above phenomenology (II), can be related to the diffusion-driven instability of a spatially homogeneous equilibrium different from P_e. In Section **6**, some concluding remarks close the paper.

2. The model

The DIB model, introduced in Bozzini *et al.* (2013) for the quantitative description of morphogenesis processes in electrodeposition, is a system of two reaction-diffusion equations, one for the morphology η (dealing with diffusion and aggregation of atoms into micro- and mesoscopic features as a continuous quantity) and one for the surface concentration θ of a crucial adsorbed chemical. The model, in adimensional form, reads as:

$$\begin{aligned} \frac{\partial \eta}{\partial t} &= \Delta\eta + \rho\, f(\eta,\theta), \\ \frac{\partial \theta}{\partial t} &= d\Delta\theta + \rho\, g(\eta,\theta), \end{aligned} \tag{1}$$

with initial conditions $\eta(x,y,0) = \eta_0(x,y), \quad \theta(x,y,0) = \theta_0(x,y), \quad (x,y) \in \Omega = [0,L_x] \times [0,L_y]$ where L_x, L_y are characteristic lengths of the electrode. Zero-flux boundary conditions are assigned on $\partial\Omega$. Here $\eta(x,y,t) \in \mathbb{R}$ expresses the displacement from the instantaneous average electrodeposit plane and can assume both negative or positive values; $0 \le \theta(x,y,t) \le 1$ is the surface coverage with the functionally crucial adsorbate; the positive parameter d accounts for diffusion, being the ratio of the diffusion coefficients for the individual chemical and morphological processes, respectively; the parameter ρ is a positive constant that can be interpreted as the relative strength of the reaction terms.

The nonlinear source terms f and g are given by

$$f(\eta,\theta) = A_1\,(1-\theta)\,\eta - A_2\eta^3 - B\,(\theta-\alpha)\,, \tag{2a}$$

$$g(\eta,\theta) = C\,(1+k_2\,\eta)\,(1-\theta)\,[1-\gamma\,(1-\theta)] - D\,[\theta\,(1+\gamma\theta)\,(1+k_3\eta)]\,, \tag{2b}$$

and account for the generation (deposition) and the loss (corrosion) of the relevant material. More precisely, in the reaction term (2a): $A_1(1-\theta)\eta$ accounts for the charge-transfer rate at sites free from adsorbates; $-A_2\eta^3$ describes mass-transport limitations to the electrodeposition process; $-B(\theta-\alpha)$ quantifies the effect of adsorbates on the electrodeposition rate; the parameter $0 < \alpha \le 1$ accounts for the fact that adsorbates can have both inhibiting and enhancing effects on the growth rate. The reaction term (2b) can be regarded as $g(\eta,\theta) = C\,g_{ads}(\eta,\theta) - D\,g_{des}(\eta,\theta)$ and features adsorption (parameter C) and desorption (parameter D) terms including both chemical and electrochemical contributions. Further details about the physico-chemical meaning of the source terms are extensively provided and discussed in Bozzini *et al.* (2013). Without loss of generality, in this work we will assume that (i) all the parameters are real positive or equal to zero, with $0 < \gamma \le 1$; (ii) $k_3 < k_2$, meaning that adsorption is the dominating chemical contribution to growth; (iii) the following relation holds:

$$D = \frac{C(1-\alpha)(1-\gamma+\gamma\alpha)}{\alpha(1+\gamma\alpha)} \tag{3}$$

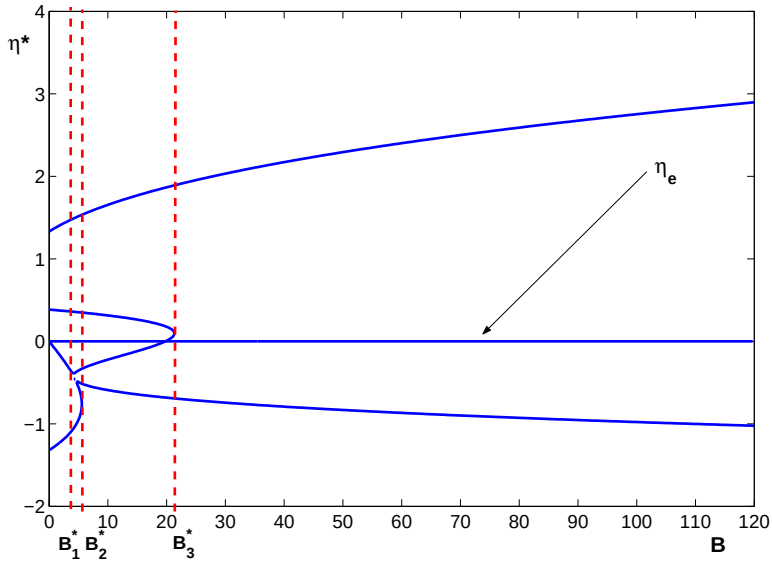

FIGURE 1. Bifurcation diagram in the (B,η^*) plane. The number of the spatially uniform equilibria (η^*,θ^*) for model (1)-(3) is shown as function of the parameter B. The other parameters are fixed as follows: $\alpha = 0.5$; $\gamma = 0.2$; $k_2 = 2.5$; $k_3 = 1.5$; $A_1 = 10$; $A_2 = 30$. The parameter C has no role in deciding the number and the numerical value of spatially uniform equilibria. Here $\theta^* = 0.5\left(20\,\eta^* - 60\,\eta^{*3} + B\right)/(10\,\eta^* + B)$. In this specific case, three threshold values B_i^* exist and there are three possible scenarios: 5 equilibria exist for $B \in (0,B_1^*) \cup (B_2^*,B_3^*)$; 7 equilibria exist for $B \in (B_1^*,B_2^*)$; 3 equilibria exist for $B > B_3^*$. We observe that $P_e = (\eta_e,\theta_e) = (0,\alpha)$ is always a spatially uniform equilibrium for the system.

implying that adsorbates enhance the growth rate and the adsorption and desorption rates are proportional ($D \propto C$).

As discussed in Lacitignola *et al.* (2015), the source terms (2) with condition (3) allow model (1) to support a multiplicity of spatially uniform equilibria. In particular, condition (3) ensures that: (i) the parameter C has no role in deciding the number and the numerical value of spatially uniform equilibria; (ii) $P_e = (\eta_e,\theta_e) = (0,\alpha)$ is a spatially independent equilibrium for any choice of all parameter values. In Figure 1 we show a bifurcation diagram in the (B,η^*) plane showing how the number of spatially uniform equilibria (η^*,θ^*) in the system can change by varying the parameter B when all the other system parameters have been fixed. Figure 1 also shows that - except for $P_e = (0,\alpha)$ - the components of the other equilibria vary with varying the parameter B. We recall that, from a physico-chemical point of view P_e corresponds to a flat electrode surface ($\eta_e = 0$) from which corrugation and morphology can develop. For this reason, the stability properties of P_e, as well as the possible mechanisms responsible for its destabilization, have a certain interest and have

been the object of investigations in Lacitignola *et al.* (2014, 2015, 2017). In the next section, we review the ways by which P_e can lose its stability both in the spatially homogeneous and in the spatial dependent case.

3. P_e's destabilization mechanisms: an overview

In the spatially independent case, linear stability analysis shows that P_e can change its stability properties because of two specific bifurcations of equilibria: a supercritical Hopf bifurcation and a transcritical one. The supercritical Hopf bifurcation occurs when P_e loses its stability and a stable limit cycle emerges surrounding the now unstable equilibrium P_e: at the bifurcation, a couple of complex conjugate eigenvalues of the Jacobian matrix $J(\eta_e,\theta_e)$ crosses the imaginary axis. The transcritical bifurcation occurs when the attracting equilibrium P_e loses its stability because it exchanges its stability properties with another equilibrium: at the bifurcation value, P_e becomes non-hyperbolic since one real eigenvalue of the related Jacobian matrix vanishes.

The Jacobian matrix $J(\eta,\theta)$ evaluated at the homogeneous steady state P_e is given by:

$$J(\eta_e,\theta_e)=\begin{bmatrix} A_1(1-\alpha) & -B \\ C(k_2-k_3)F_1(\alpha,\gamma) & -CF_2(\alpha,\gamma) \end{bmatrix}, \tag{4}$$

where

$$F_1(\alpha,\gamma)=(1-\alpha)(1-\gamma+\alpha\gamma); \qquad F_2(\alpha,\gamma)=\frac{2\alpha\gamma(1+\alpha\gamma-\gamma)+1-\gamma}{\alpha(1+\alpha\gamma)}. \tag{5}$$

Denoting with $\tau_e=\mathrm{tr}(J(\eta_e,\theta_e))$ and $\delta_e=\det(J(\eta_e,\theta_e))$, the Hopf bifurcation can be detected by requiring $\tau_e=0$ and $\delta_e>0$ that, in terms of the bifurcation parameters, gives the threshold values:

$$C=C_{hopf}=A_1(1-\alpha)F_2(\alpha,\gamma)^{-1}, \qquad B>B_{tr}=A_1(1-\alpha)F_2(\alpha,\gamma)\left[(k_2-k_3)F_1(\alpha,\gamma)\right]^{-1}.$$

Here B_{tr} is the threshold value for the occurrence of a transcritical bifurcation that can be detected by requiring $\delta_e=0$. In Figure 2, we show the two-parameter bifurcation diagram in the parameter space (C,B), for a specific choice of the other parameter values: the vertical line $C=C_{hopf}$ and the horizontal line $B=B_{tr}$ are the Hopf and transcritical bifurcations lines, respectively. In the region to the right of the Hopf line and above the transcritical line, the homogeneous equilibrium P_e is unconditionally stable in the non-spatial case as $\tau_e<0$ and $\delta_e>0$. By choosing parameters below the transcritical bifurcation line, $\delta_e<0$ holds, so that P_e can be destabilized by small homogeneous perturbations and system trajectories tend toward a different stable steady state. In the region above the transcritical line and on the left of the Hopf one, P_e is unstable so that homogeneous oscillations emerge as a consequence of a supercritical Hopf bifurcation. In Figure 3, we show the phase plane portrait depicting the oscillatory system dynamics for different choices of the parameter $C<C_{hopf}$. A proof of the supercritical nature of the Hopf bifurcation has been provided in Lacitignola *et al.* (2015). In the spatial dependent case, linear stability analysis enables to prove that P_e undergoes (Turing) diffusion-driven instability, that is responsible for the emergence of spatial patterns for system (1)-(2). As widely known in literature, a reaction-diffusion system is said to exhibit diffusion-driven instability if a spatially uniform steady state - that is locally *stable*

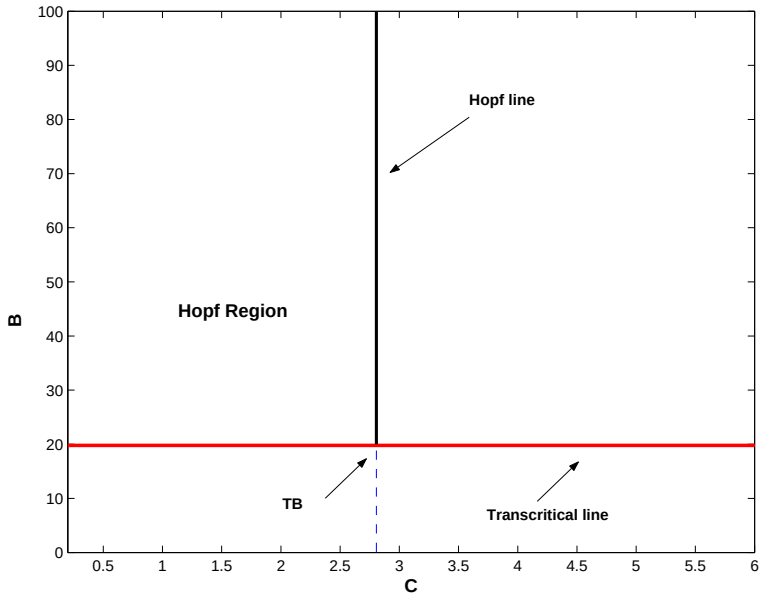

FIGURE 2. The non spatial case. Bifurcation diagram in the parameter space (C,B) related to the stability properties of the equilibrium P_e. The other parameters are fixed as in Figure 1. $C = C_{hopf} = 2.8061$ is the Hopf bifurcation line; $B = B_{tr} = 19.7979$ is the transcritical line. The bifurcation point TB where the transcritical and Hopf lines meet is $(C_{TB}, B_{TB}) = (2.8061, 19.7979)$.

in the absence of diffusion - becomes *unstable* to small spatial perturbations when diffusion is present (Murray 2003).

For the general system (1)-(2), the P_e's Turing parameter space - consisting of parameters resulting in Turing instability for P_e - is bounded by the following inequalities:

$$J^e_{11} + J^e_{22} < 0, \quad J^e_{11}J^e_{22} - J^e_{12}J^e_{21} > 0, \quad dJ^e_{11} + J^e_{22} > 0, \quad (J^e_{22} + dJ^e_{11})^2 > 4d\,\delta_e, \tag{6}$$

where J^e_{ij} stands for the ij entry of the Jacobian matrix $J(P_e)$ evaluated at the equilibrium $P_e = (\eta_e, \theta_e)$. The first two inequalities are derived by stability considerations on the homogeneous equilibrium P_e in the absence of diffusion, the others are obtained by considerations on the onset of instability when diffusion is introduced. Chosen B and C as bifurcation parameters, the set of conditions (6) specializes as:

$$\begin{cases} \dfrac{A_1(1-\alpha)}{F_2(\alpha,\gamma)} < C < \dfrac{dA_1(1-\alpha)}{F_2(\alpha,\gamma)}, \\ B > \dfrac{A_1(1-\alpha)F_2(\alpha,\gamma)}{(k_2-k_3)F_1(\alpha,\gamma)}, \\ B < \dfrac{d^2A_1^2(1-\alpha)^2 + CF_2(\alpha,\gamma)\,[2A_1d(1-\alpha) + CF_2(\alpha,\gamma)]}{4dC(k_2-k_3)F_1(\alpha,\gamma)}, \end{cases} \tag{7}$$

with $d > 1$ and $dA_1(1-\alpha) \neq CF_2(\alpha,\gamma)$. Inequalities (7) define a region in the parameter space such that P_e is stable to small perturbations in the absence of diffusion, but it can be

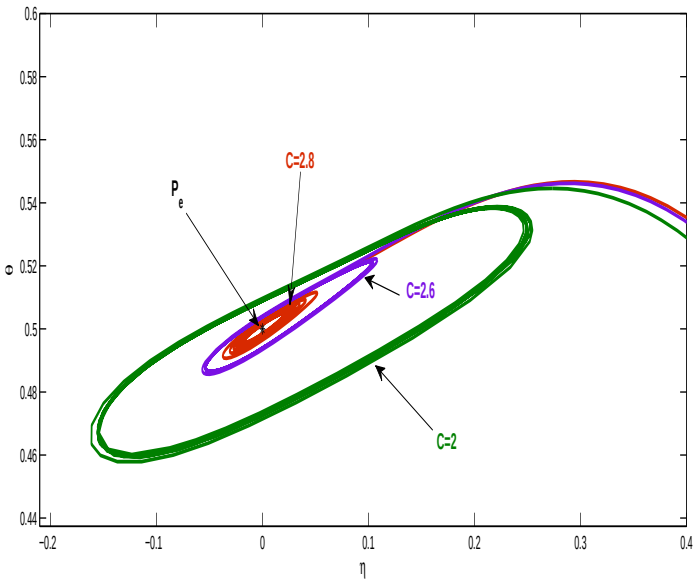

FIGURE 3. The non spatial case. Oscillatory dynamics near the supercritical Hopf bifurcation at $C_{Hopf} = 2.8061$. Phase portraits of the stable limit cycles surrounding P_e, obtained for $B = 22$ and different values of $C < C_{Hopf}$. The other system parameters are set as in Figure 1.

unstable to small spatial perturbations when the diffusion is not neglected. In this region of the parameter space, the formation of stationary spatial patterns is hence expected because of the interaction between the nonlinear reaction terms and the diffusion process.

In Figure 4 we show the P_e's Turing region in the parameter space (C,B) for a fixed value of the diffusion parameter $d = 20$. The points where different bifurcation curves meet correspond to bifurcations of higher codimension that can be related to the emergence of complex spatio-temporal dynamics. More precisely, the transcritical and the Turing bifurcation curves meet at the point TT, whose coordinates are

$$C_{TT} = \frac{dA_1(1-\alpha)}{F_2(\alpha,\gamma)}; \qquad B_{TT} = \frac{A_1(1-\alpha)F_2(\alpha,\gamma)}{(k_2-k_3)F_1(\alpha,\gamma)};$$

the transcritical and the Hopf lines meet at the codimension-two bifurcation point TB, whose coordinates are

$$C_{TB} = \frac{A_1(1-\alpha)}{F_2(\alpha,\gamma)}; \qquad B_{TB} = \frac{A_1(1-\alpha)F_2(\alpha,\gamma)}{(k_2-k_3)F_1(\alpha,\gamma)};$$

the Hopf and Turing bifurcation curves meet at codimension-two bifurcation point TH, whose coordinates are

$$C_{TH} = \frac{A_1(1-\alpha)}{F_2(\alpha,\gamma)}; \qquad B_{TH} = \frac{A_1(1-\alpha)F_2(\alpha,\gamma)(1+d)^2}{4d(k_2-k_3)F_1(\alpha,\gamma)}.$$

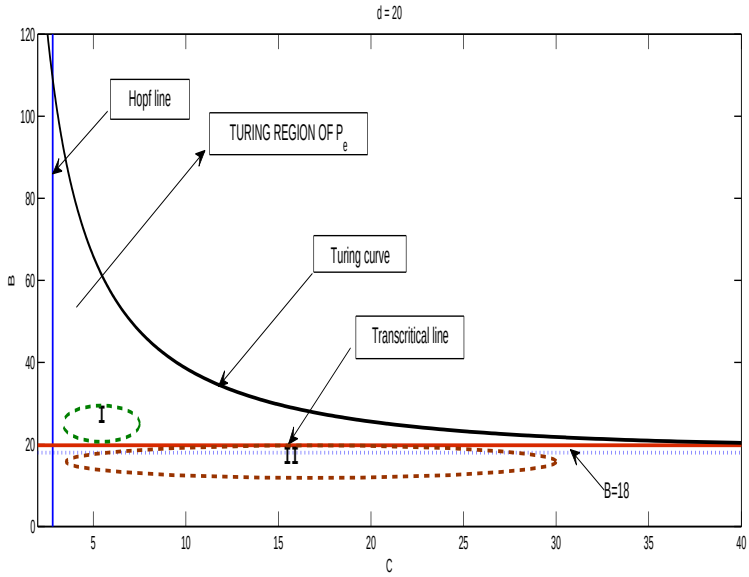

FIGURE 4. P_e's Turing region in the (C,B) parameter space for $d = 20$. The other parameters are fixed as in Figure 1. The Turing region of P_e in the parameter space (C,B) is bounded by the Hopf line $C = C_{Hopf}$, the trancritical line $B = B_{tr}$ and the Turing bifurcation curve. For this choice of the parameter values, the codimension-two bifurcation points TH and TB have coordinates $(C_{TH},B_{TH}) = (2.8061,109.13)$ and $(C_{TB},B_{TB}) = (2.8061,19.7979)$. The dashed below the transcritical bifurcation line is the line $B = 18$ that we have drawn for a comparison with the two-parameter bifurcation diagram in Figure 7. Region I qualitatively represents that portion in the P_e's Turing parameter space where the phenomenology (I) can be observed. Region II, outside the P_e's Turing Region and just below the transcritical bifurcation line, is instead associated to the phenomenology (II).

In particular the points TB and TH are interesting for the search of potentially complex dynamics. In fact, in the neighboring of TB a Takens-Bogdanov bifurcation can occur that can be usually related to the existence of homoclinic bifurcations and to emergence of complex spatio-temporal behaviors; in the neighborhood of the TH point, the formation of inhomogeneous stationary patterns caused by Turing instabilities, interacts with the appearance of homogeneous oscillations due to a Hopf bifurcation and this intriguing interplay is responsible for the emergence of an interesting class of spatio-temporal patterns. This last mechanism and the resulting phenomenology has been investigated in details in Lacitignola *et al.* (2015).

To conclude this overview, we recall that in the P_e's Turing parameter space, according to the specific values of the bifurcation parameter B and C, different typologies of Turing patterns can be found. In particular, the bifurcation parameter B turns out to have a clear

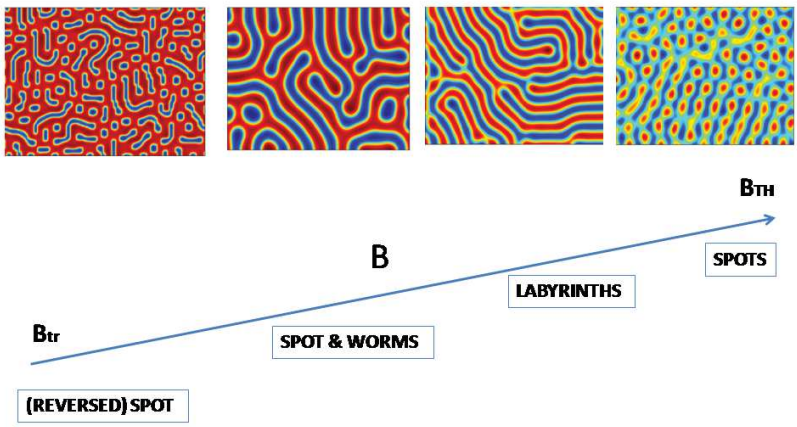

FIGURE 5. The pattern selection problem. Qualitative sketch of the morphological classes of spatial patterns obtained in the interior of the P_e's Turing parameter space for increasing values of the parameter $B \in (B_{tr}, B_{TH})$. The reader is referred to Lacitignola *et al.* (2015) for a more detailed characterization of the Turing morphological classes.

role in the pattern selection problem. By fixing the value of C in the Turing parameter space and progressively increasing the value of the bifurcation parameter $B \in (B_{tr}, B_{TH})$, it is possible to observe that for $B > \approx B_{tr}$ patterns of (reversed) spots appear, corresponding to holes in a uniform flat morphology; further increasing the values of B patterns of spots and worms appear that, for even higher values of B, turn into a more connected labyrinthine-like structure. When the value of B is further increased and approaches the neighborhood of the point TH, the labyrinthine-like structure breaks down yielding a stationary tessellation pattern of spots (Lacitignola *et al.* 2015). In Figure 5, a qualitative sketch is shown of the different morphological classes of spatial patterns for the DIB model, obtained in the P_e's Turing parameter space, for increasing values of the parameter $B \in (B_{tr}, B_{TH})$ (Lacitignola *et al.* 2015).

In the next section we show that the existence of Region I, associated to the phenomenology (I) we described in Section **1**, is related to the peculiar role of the parameter A_2 on the system dynamics.

4. The role of the parameter A_2 on the system dynamics

To elucidate the role of the parameter A_2, we first observe that the bifurcation thresholds of the spatially homogeneous equilibrium P_e do not depend on the parameter A_2, so that the

two-parameter bifurcation diagram in Figure 4, which regards the different ways in which P_e can lose its stability, remains unchanged.

However, as already observed in Lacitignola *et al.* (2015), the parameter A_2 seems to have a certain impact on the features of the spatial patterns in the P_e's Turing parameter space and an interesting role in the pattern selection problem. In fact, low values of A_2 cause a disruption of the labyrinthine structure resulting in reversed spots, that is holes in a homogeneous flat morphology. Moreover, numerical simulations in Sgura *et al.* (2018) have recently shown that a subregion in the P_e's Turing parameter space exists where no stationary spatial patterns can be found since system dynamics tend towards a spatially homogeneous equilibrium, different from P_e. Such a subregion, that is just above the transcritical line (Region I in Figure 4), enlarges for lower values of the parameter A_2; it becomes thinner and thinner when A_2 is increased and then disappears for sufficiently high values of A_2.

This kind of phenomenology within the P_e's Turing parameter space can be completely explained by looking at the role that A_2 has on the existence and stability properties of some spatially uniform equilibria of the DIB model. In order to show that, in Figure 6 we present the (B, θ^*) bifurcation diagram of the *feasible* (i.e. $0 < \theta < 1$) spatially uniform equilibria, obtained for a low ($A_2 = 1$) and a high ($A_2 = 30$) value of the parameter A_2. We recall that for the chosen values of the parameters, in the P_e's Turing parameter space $19.7979 < B < 109.13$. In both the cases $A_2 = 1$ and $A_2 = 30$, two relevant bifurcations of the spatially homogeneous equilibria can be observed in the system when diffusion is switched off: (i) a transcritical bifurcation, at $B = B_{tr}$, which consists in the exchange of stability properties between the equilibria P_e and P_1 so that P_e is unstable for $B < B_{tr}$ and becomes stable for $B > B_{tr}$ whereas P_1 has the opposite behavior; (ii) a saddle-node bifurcation at $B = B_{SN}$ where the unstable equilibrium P_1 and the stable equilibrium P_2 coalesce and then disappear for $B > B_{SN}$. Therefore, for $B \in (B_{tr}, B_{SN})$, it can be found a Region I in the P_e's Turing parameter space where the reaction-diffusion system tends to a spatially homogeneous equilibrium. The size of this subregion is strongly related to the width of the range (B_{tr}, B_{SN}), namely the range where the equilibrium P_e (which is stable in absence of diffusion and becomes unstable when diffusion is switched on) coexists with the stable equilibrium P_2. Choosing the values of B in this range, one has that - according to the initial conditions - the asymptotic system outputs can be either a Turing pattern due to the diffusion-driven instability of P_e or the spatially homogeneous equilibrium P_2. In fact, for $B \in (B_{tr}, B_{SN})$, the three equilibria P_e, P_1, P_2 have quite similar numerical values so that, when diffusion is present and P_e is diffusion-driven unstable, initial conditions in the neighboring of P_e can also drive the system trajectories towards the stable equilibrium P_2. Figure 6 also shows that the width of the range (B_{tr}, B_{SN}) is strongly influenced by the parameter A_2 since - although the transcritical bifurcation threshold does not change with changing A_2 - the saddle-node bifurcation threshold B_{SN} depends upon A_2 and becomes larger for smaller values of this parameter. This means that lower values of the parameter A_2 will correspond to a larger range (B_{tr}, B_{SN}), hence allowing for a larger basin of attraction of the spatially homogeneous equilibrium P_2. As a consequence, a larger Region I within the P_e's Turing parameter space can be detected, where the system can tend towards P_2 rather than towards a Turing spatial pattern. In the next section, we explain the occurrence of the phenomenology (II), described in Section **1**, for which stationary spatial patterns can be

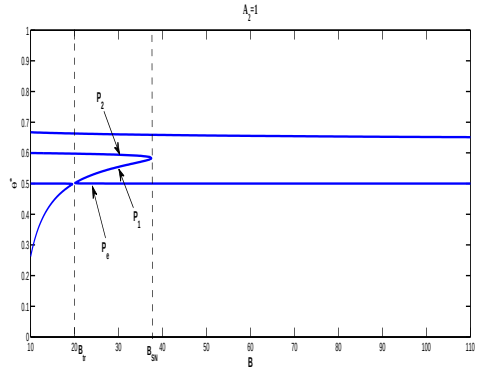

(a)

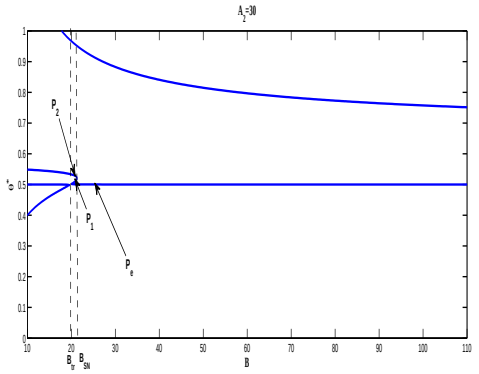

(b)

FIGURE 6. (B, θ^*) bifurcation diagram of the *feasible* (i.e. $0 < \theta < 1$) spatially uniform equilibria of the DIB model. (a) The case $A_2 = 1$. The transcritical threshold is $B_{tr} = 19.7979$ and the saddle-node bifurcation threshold is $B_{SN} = 37.5755$. Hence, according to the initial conditions, for $19.8 < B < 37.5755$ the system can tend towards the Turing patterns due to the diffusion-driven instability of P_e or towards the spatially homogeneous equilibrium P_2 whose θ's component varies from $\theta = 0.5975$ (when $B = 19.8$) to $\theta = 0.5830$ (when $B = 37.5755$). For $B > B_{SN} = 37.5755$ and initial conditions in the neighboring of P_e, the system tend towards Turing spatial patterns. (b) The case $A_2 = 30$. The transcritical threshold is $B_{tr} = 19.7979$ and the saddle-node bifurcation threshold is $B_{SN} = 21.3356$. For $19.8 < B < 21.3356$, the system can tend towards the Turing patterns due to the diffusion-driven instability of P_e or to the spatially homogeneous equilibrium P_2 whose θ's component varies from $\theta = 0.5337$ (when $B = 19.8$) to $\theta = 0.52045$ (when $B = 21.3356$). For $B > B_{SN} = 21.3356$ and initial conditions in the neighboring of P_e, Turing spatial patterns are the only output for the system.

found also outside the P_e's Turing parameter space, in a region just below the transcritical bifurcation threshold.

5. On some spatial patterns outside the P_e's Turing Region

In this section we show that the phenomenology (II) - qualitatively associated to Region II in Figure 4 - is linked to the fact that, for $B < B_{tr}$ (where P_e is unstable), the stable spatially homogeneous equilibrium P_1 can loose its stability because of the diffusion-driven instability phenomenon, therefore leading to the emergence of spatial patterns below the transcritical bifurcation line $B = B_{tr}$ of Figure 4. To clarify this point, we analyze in more details the case $B < B_{tr}$. By fixing the parameter values as in Figure 4, we have that the transcritical bifurcation threshold is $B = B_{tr} = 19.7979$. We hence consider $B = 18$ as representative of the case $B < B_{tr}$ and let C and d to be bifurcation parameters. For the chosen set of parameter values, the three equilibria involved in the transcritical and in the saddle-node bifurcations have the following coordinates: $P_e = (0, 0.5)$, $P_1 = (-0.0512, 0.4858)$, $P_2 = (0.2205, 0.5386)$. When diffusion is neglected, we know by Section **3** that the equilibrium P_e is unstable; linear stability analysis easily shows that the equilibrium P_1 is stable for $C > 3.0780$ and that the equilibrium P_2 is stable for $C > 0.0920$. When diffusion is switched on, it is possible to show that both P_1 and P_2 can undergo Turing instability. The related Turing Regions in the parameter space (C, d) are shown in Figure 7. In order to set the results found in this section within the framework of the two-parameter bifurcation diagram in Figure 4 we observe that, when $d = 20$ and $B = 18$, we are on the dashed line just below the transcritical bifurcation line in Figure 4. From Figure 7 it clearly appears that, in the (C, d) parameter space, the Turing region of P_2 is extremely narrow and the emergence of spatial patterns is only allowed for values of d such that $d > 39.25$. Hence, for $d = 20$, no spatial patterns can emerge because the Turing instability of P_2. On the contrary, in the (C, d) parameter space, the Turing region of P_1 is extremely wide and, for $d = 20$, spatial patterns are allowed for values of C such that $3.07807 < C < 31.451441$. Therefore, the Turing instability of the spatially homogeneous equilibrium P_1 can be responsible for the emergence of spatial patterns outside the P_e's Turing parameter space, in the Region II of the two-parameter bifurcation diagram in Figure 4.

6. Concluding remarks

This study wants to be a further step of the mathematical inquiry into the rich spatio-temporal dynamics of the DIB model. Previous studies on this model have essentially related its capability to support spatial patterns to the different mechanisms of destabilization of a specific equilibrium of the system, the equilibrium P_e: P_e was shown to undergo diffusion-driven instability and the resulting P_e's Turing parameter space was shown to exhibit different classes of morphological stationary spatial patterns such as spots, reversed spots, spots and worms, labyrinths (Lacitignola *et al.* 2015). However a certain subregion of the P_e's Turing parameter space have been found, where the emergence of spatial patterns seems to be inhibited and system trajectories tend towards a spatially homogeneous equilibrium. Moreover spatial patterns have been observed also outside the P_e's Turing parameter space (Sgura *et al.* 2018).

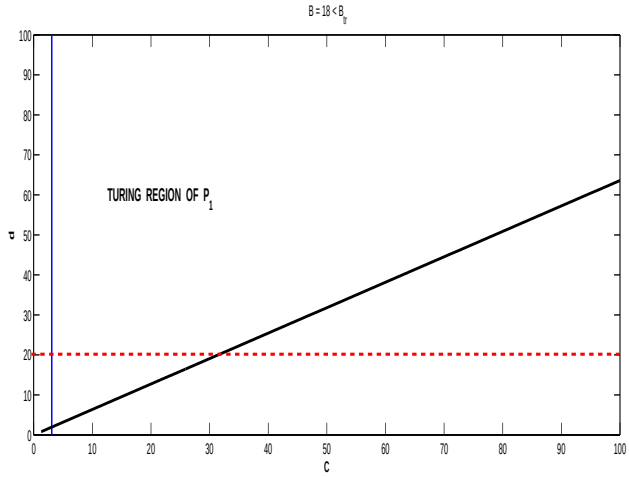

(a)

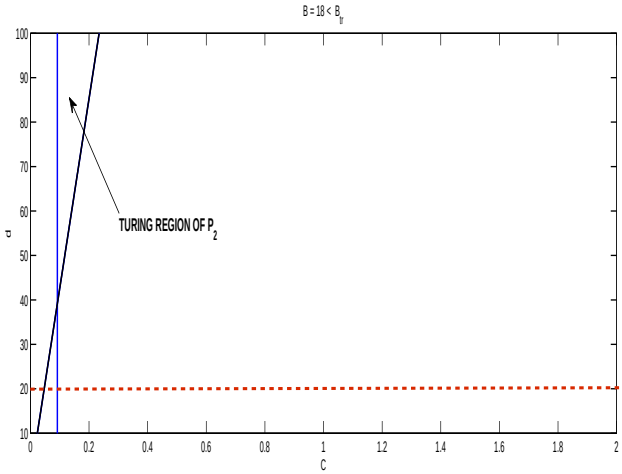

(b)

FIGURE 7. The case $B < B_{tr} = 19.7979$. Bifurcation diagram in the parameter space (C,d) for the case $B = 18$. The values for the other parameters are as in Figure 1. The dashed (red line) is the line $d = 20$ that we have drawn for a comparison with the two-parameter bifurcation diagram in Figure 4. (Left panel) Turing parameter space (C,d) of the spatially homogeneous equilibrium $P_1 = (-0.0512, 0.4855)$. (Right panel) Turing parameter space (C,d) of the spatially homogeneous equilibrium $P_2 = (0.2205, 0.5386)$.

In this study, we have shown that these dynamical behaviors can be explained and characterized in terms of several bifurcations involving some of the many equilibria of the DIB model. This feature well puts into evidence the potential richness that the presence of multiple equilibria can add to the dynamical scenarios and to the spatio-temporal dynamics of a given system. Moreover, the findings developed in this study also suggest the importance of further investigations on other possible mechanisms, different from the Turing one, that could be responsible for pattern formation in this morphochemical model for metal growth. This would allow for a broader and deeper understanding of the different spatio-temporal dynamics that the DIB model can support in the different regions of the parameters space.

Acknowledgments

The present work has been performed under the auspices of the Italian National Group for Mathematical Physics (GNFM-Indam). The author sincerely wishes to thank the Scientific and Organizing Committees for the kind invitation and the warm hospitality during the International *School & Research Workshop M.M.SE.OR. 2017* in Giardini Naxos (Messina, Italy).

References

Bozzini, B., Gambino, G., Lacitignola, D., Lupo, S., Sammartino, M., and Sgura, I. (2015). "Weakly nonlinear analysis of Turing patterns in a morphochemical model for metal growth". *Computers & Mathematics with Applications* **70**(8), 1948–1969. DOI: 10.1016/j.camwa.2015.08.019.

Bozzini, B., Lacitignola, D., and Sgura, I. (2013). "Spatio-temporal organization in alloy electrodeposition: a morphochemical mathematical model and its experimental validation". *Journal of Solid State Electrochemistry* **17**(2), 467–479. DOI: 10.1007/s10008-012-1945-7.

Cross, M. and Greenside, H. (2009). *Pattern Formation and Dynamics in Nonequilibrium Systems*. Cambridge University Press. DOI: 10.1017/CBO9780511627200.

De Wit, A. (1999). "Spatial patterns and spatiotemporal dynamics in chemical systems". *Adv. Chem. Phys.* **109**, 435–513. DOI: 10.1002/9780470141687.ch5.

Epstein, J. (1997). *Nonlinear Dynamics, Mathematical Biology and Social Science*. Boca Raton: CRC Press.

Kapral, R. and Showalter, K. (1995). *Chemical Waves and Patterns*. Kluwer Academic Publishers. DOI: 10.1007/978-94-011-1156-0.

Lacitignola, D., Bozzini, B., Frittelli, M., and Sgura, I. (2017). "Turing pattern formation on the sphere for a morphochemical reaction-diffusion model for electrodeposition". *Communications in Nonlinear Science and Numerical Simulation* **48**, 484–508. DOI: 10.1016/j.cnsns.2017.01.008.

Lacitignola, D., Bozzini, B., Peipmann, R., and Sgura, I. (2018). "Cross-diffusion effects on a morphochemical model for electrodeposition". *Applied Mathematical Modelling* **57**, 492–513. DOI: 10.1016/j.apm.2018.01.005.

Lacitignola, D., Bozzini, B., and Sgura, I. (2014). "Spatio-Temporal Organization in a Morphochemical Electrodeposition Model: Analysis and Numerical Simulation of Spiral Waves". *Acta Applicandae Mathematicae* **132**, 377–389. DOI: 10.1007/s10440-014-9910-3.

Lacitignola, D., Bozzini, B., and Sgura, I. (2015). "Spatio-Temporal Organization in a Morphochemical Electrodeposition Model: Hopf and Turing instabilities and their interplay". *European Journal of Applied Mathematics* **26**(2), 143–173. DOI: 10.1017/S0956792514000370.

Maini, P. and Othmer, H. (2001). *Mathematical Models for Biological Pattern Formation. The IMA Volumes in Mathematics and its Applications - Frontiers in Applications of Mathematics, Vol. 121*. Springer-Verlag New York. DOI: 10.1007/978-1-4613-0133-2.

Malchow, H., Petrovski, S., and Venturino, E. (2008). *Spatiotemporal Patterns in Ecology and Epidemiology:Theory, Models, and Simulation*. Chapman & Hall U.K.

Murray, J. (2003). *Mathematical Biology II - Spatial Models and Biomedical Applications*. Springer-Verlag Berlin Heidelberg. DOI: 10.1007/b98869.

Sgura, I., Lawless, A. S., and Bozzini, B. (2018). "Parameter estimation for a morphochemical reaction-diffusion model of electrochemical pattern formation (in press)". *Inverse Problems in Science and Engineering*, 1–30. DOI: 10.1080/17415977.2018.1490278.

Sherratt, J. (2012). *Turing patterns in deserts. In:* How the World Computes*, ed. S.B. Cooper, A. Dawar, B. Lowe, Lecture Notes in Computer Science 7318*. Springer New York. DOI: 10.1007/978-3-642-30870-3_67.

Turing, A. M. (1952). "The Chemical Basis of Morphogenesis". *Philosophical Transactions of the Royal Society of London B: Biological Sciences* **237**(641), 37–72. DOI: 10.1098/rstb.1952.0012.

Vanag, V. K. (2004). "Waves and patterns in reaction-diffusion systems.Belousov-Zhabotinsky reaction in water-in-oil microemulsions". *Physics-Uspekhi* **47**(9), 923–941. DOI: 10.1070/PU2004v047n09ABEH001742.

* Università degli Studi di Cassino e del Lazio Meridionale
Dipartimento di Ingegneria Elettrica e dell'Informazione
Via Di Biasio, 03043 Cassino, Italy

Email: d.lacitignola@unicas.it

Paper contributed to the workshop entitled "Mathematical modeling of self-organizations in medicine, biology and ecology: from micro to macro", which was held at Giardini Naxos, Messina, Italy (18–21 September 2017)
under the patronage of the *Accademia Peloritana dei Pericolanti*
Manuscript received 9 April 2018; published online 30 November 2018